HYDROLOGICAL PROCESSES
Hydrol. Process. (2012)
Published online in Wiley Online Library
(wileyonlinelibrary.com) DOI: 10.1002/hyp.9549

Aspect control of water movement on hillslopes near the rain–snow transition of the Colorado Front Range

Eve-Lyn S. Hinckley,[1,2]* Brian A. Ebel,[3] Rebecca T. Barnes,[4] Robert S. Anderson,[1,5]
Mark W. Williams[1,6] and Suzanne P. Anderson[1,6]

[1] *Institute of Arctic and Alpine Research, Boulder, CO, 80309 USA*
[2] *The National Ecological Observatory Network, Boulder, CO, 80301 USA*
[3] *United States Geological Survey, Boulder, CO, 80303 USA*
[4] *Bard Center for Environmental Policy, Bard College, Annandale-on-Hudson, NY, 12504 USA*
[5] *Department of Geological Sciences, University of Colorado, Boulder, CO, 80309 USA*
[6] *Department of Geography, University of Colorado, Boulder, CO, 80309 USA*

Abstract:

In the Colorado Front Range, forested catchments near the rain–snow transition are likely to experience changes in snowmelt delivery and subsurface water transport with climate warming and associated shifts in precipitation patterns. Snowpack dynamics are strongly affected by aspect: Lodgepole pine forested north-facing slopes develop a seasonal snowpack, whereas Ponderosa pine-dotted south-facing slopes experience intermittent snow accumulation throughout winter and spring. We tested the degree to which these contrasting water input patterns cause different near-surface hydrologic response on north-facing and south-facing hillslopes during the snowmelt period. During spring snowmelt, we applied lithium bromide (LiBr) tracer to instrumented plots along a north–south catchment transect. Bromide broke through immediately at 10- and 30-cm depths on the north-facing slope and was transported out of soil waters within 40 days. On the south-facing slope, Br^- was transported to significant depths only during spring storms and remained above the detection limit throughout the study. Modelling of unsaturated zone hydrologic response using Hydrus-1D corroborated these aspect-driven differences in subsurface transport. Our multiple lines of evidence suggest that north-facing slopes are dominated by connected flow through the soil matrix, whereas south-facing slope soils experience brief periods of rapid vertical transport following snowmelt events and are drier overall than north-facing slopes. These differences in hydrologic response were largely a function of energy-driven differences in water supply, emphasizing the importance of aspect and climate forcing when considering contributions of water and solutes to streamflow in catchments near the snow line. Copyright © 2012 John Wiley & Sons, Ltd.

KEY WORDS lithium bromide tracer; slope aspect; temperature-index model; Hydrus-1D; critical zone; Boulder Creek Critical Zone Observatory

Received 25 October 2011; Accepted 20 August 2012

INTRODUCTION

Spring snowmelt is the major hydrologic event supplying water to high elevation terrestrial ecosystems at mid-latitudes in the Western Hemisphere. This water is critical for recharging soil moisture reserves, sustaining vegetation, and feeding stream networks. One of the major gaps in our understanding of how melt water is partitioned into infiltration, evapotranspiration, groundwater recharge, and overland flow is lack of knowledge of the connections between snowpack dynamics and the evolution of hydrological flow paths during the melt season (Bales *et al*., 2006; Molotch *et al*., 2009; Williams *et al*., 2009a). Altered precipitation patterns and warming temperatures from climate shifts could potentially change the timing and subsurface flow paths of melt water inputs (Clow, 2010). These impacts will increase the risk of prolonged droughts in already water-limited systems and potentially cause secondary effects, such as higher incidences of disease and fire (Hogg and Hurdle, 1995), altered biogeochemical cycling of nitrogen (N) and carbon (C) (e.g. Williams *et al*., 1998; Steinweg *et al*., 2008), and changes in vegetation communities (Molotch *et al*., 2009).

Several research efforts have focused on understanding snowpack accumulation, melt, and associated runoff in alpine ecosystems (Greenland, 1989; Liu *et al*., 2004) and sub-alpine systems (e.g. Molotch *et al*., 2009; Williams *et al*., 2009b), which experience one primary snowmelt event per year. In western North America, the snowpack begins to accumulate in November and typically reaches its maximum in May (Erickson and Williams, 2005); in the Rocky Mountains, USA, ~85% of water inputs are snow (Stewart *et al*., 2004). However, recent studies in the Rocky Mountain headwaters region have shown that higher temperatures may shift the timing of maximum snow accumulation to earlier and decrease the proportion of snow relative to rain (e.g. Rood *et al*., 2008). In general, most of the research in these systems have related melt water contribution to soil moisture reserves and vegetation water use but not explicitly studied the simultaneous evolution of subsurface hydrological flow paths.

*Correspondence to: Eve-Lyn S. Hinckley, The National Ecological Observatory Network, Boulder, CO, 80301 USA
E-mail: ehinckley@neoninc.org

Few studies have focused on snowmelt and transport in lower elevation systems where snowpack may be intermittent in the winter and spring. In these environments, near-surface hydrologic response and connectivity to the channel are commonly both spatially and temporally variable (Haught and van Meerveld, 2011; Phillips *et al.*, 2011). Understanding the timing and rate of melt water flux into soils is particularly important in these systems because they are likely to change dramatically in response to climatic shifts, for example, temperature increases that could cause precipitation phase changes and changes in snowmelt timing (e.g. Clow, 2010; Williams *et al.*, 2009a). In one study, McNamara *et al.* (2005) described annual soil moisture storage characteristics in an arid catchment at the rain–snow transition in Idaho. The five-state model includes (1) summer dry, (2) transitional fall wetting, (3) winter wet, low flux, (4) spring wet, high flux, and (5) transitional late-spring drying. As the system transitioned from dry to wet, McNamara *et al.* (2005) observed a change in the dominant flow path of water from vertical to lateral flow, which was largely controlled by hydraulic soil properties and the rate of water delivery to the soil. This detailed view of catchment moisture states was preceded by the work of Grayson *et al.* (1997) and Stieglitz *et al.* (2003) that described a two-state mode in catchments: dry, unconnected and wet, connected.

Building on the study by McNamara *et al.* (2005), we investigate the role that aspect plays in determining moisture states and hydrologic flow paths at the rain–snow transition. We chose to evaluate the timing, flux, and subsurface fates of snowmelt at the rain–snow transition in the Colorado Front Range of the Rocky Mountains. The Rocky Mountains run north–south and are drained by east–west trending valleys, producing predominately north-aspect and south-aspect slopes. This difference in aspect affects patterns of snowpack accumulation and melt, particularly at altitudes with a marginal seasonal snowpack: a persistent snowpack develops on north-facing slopes, whereas snowpack is intermittent on south-facing slopes. Following these expected patterns of snow accumulation, we hypothesized that melt water delivery is controlled by environmental conditions (e.g. air temperature and wind) on north-facing slopes and by the presence of snow on south-facing slopes. In addition, we hypothesized that differences in melt water delivery would determine near-surface hydrologic response and soil-water storage (e.g. Broxton *et al.*, 2009; Geroy *et al.*, 2011; Smith *et al.*, 2011): tree-covered north-facing slopes with deeper soils would promote infiltration into the soil matrix and store melt water into the summer growing season, whereas more open, grass-covered south-facing slopes with shallower soils would experience pronounced wetting and drying cycles between snow storms, with drier soils at the onset of the summer growing season.

We conducted lithium bromide (LiBr) tracer studies during the 2010 snowmelt season to understand the effects of aspect on near-surface hydrological flow paths. Measurements of soil-water content and soil temperature were used to understand the timing of soil thawing and subsurface hydrologic dynamics in response to snowmelt fluxes. In addition, we estimated water delivery from snowmelt and soil-water fluxes by driving a 1D (i.e. vertical) unsaturated zone flow model with a point model of melt water flux. We conducted this study at the plot scale (i.e. point scale), in order to examine the effects of aspect at multiple points along the hillslope profiles.

STUDY AREA

Our research site is Gordon Gulch (40.01°N, 105.47°W), a 2.7-km^2 focal study sub-catchment within the Boulder Creek Critical Zone Observatory (BcCZO) in Colorado, USA. The sub-catchment is located on the Rocky Mountain surface, a low relief, high elevation region flanking the crest of the Colorado Front Range. The Rocky Mountain surface is above canyons cut by river incision during the late Cenozoic and below the limits of the Pleistocene glaciation. It has evolved with minimal tectonic perturbation since the end of the Laramide orogeny, approximately 40 Ma (Anderson *et al.*, 2006). As a result, the depth to the weathering front is significant, as deduced from seismic refraction studies (Befus *et al.*, 2011) and logs from approximately 540 water wells (Dethier and Lazarus, 2006); it averages 8 m and up to 30 m in some parts of the catchment. The bedrock is dominantly Paleoproterozoic biotite gneiss (Cole and Braddock, 2009).

At 2440–2730-m elevation, Gordon Gulch sits at the current rain–snow transition, which has been described in previous research by Williams *et al.* (2011). It develops a seasonal snowpack on north-facing slopes and an intermittent snowpack on south-facing slopes. Mean annual precipitation is 506 mm, based on the 20-year average (NADP station CO94 at 39.99°N, 105.48°W; NADP, 2011), and mean annual air temperature is 6.9 °C (WRCC, 2011). Vegetation is characteristic of the upper montane zone described by Marr (in Birkeland *et al.*, 2003). North-facing slopes are dominated by moderately dense Lodgepole pine (*Pinus contorta*), whereas low-density Ponderosa pines (*Pinus ponderosa*) dot the south-facing slopes, with intervening grasses (Peet, 1981).

Soils are primarily Bulwark–Catamount families–Rubble land complex with 5% to 40% slopes and cobbly or stony sandy loam to approximately 1.2 m in a typical profile (USDA, 2009). Along the study transect discussed below, we found that depth to saprolite on hillslopes was typically 30–35 cm and 40–45 cm on south-facing and north-facing slopes, respectively. The depth to saprolite is relatively uniform along each hillslope profile, with the exception of the toeslope (i.e. stream terrace in the riparian zone), a depositional area, where depth to saprolite is >1.5 m.

METHODS

Experimental design and hydrological observations

We established experimental plots across a north–south trending cross section of the study catchment. Plot locations included upper (U) and lower (L) positions on

DOI: 10.1002/hyp

the north-facing (NF) and south-facing (SF) aspects, as well as the toeslope (TS) adjacent to the creek (Figure 1). Each plot ($n = 1$ per hillslope position) was 4 m × 4 m, and its location was chosen for representative vegetation cover and subsurface structure, as determined by vegetation sampling and soil pit excavations completed in August 2009 (unpublished data).

Within each plot we installed instrumentation at multiple depths through the soil profile, including tension (Prenart Equipment, ApS) and zero-tension lysimeters (dimensions 10 (W) × 31 (L) × 5 (D) cm; design described in Hinckley *et al.*, 2008), soil temperature, and soil-water content sensors (Campbell Scientific model numbers CS-107 and 616, respectively). Tension lysimeters were installed in a diagonal borehole and grouted in place with silica slurry. Zero-tension lysimeters were emplaced laterally from a trench. We installed the two types of lysimeters so that we could potentially sample different flow paths of water: water moving within the soil matrix using the tension lysimeters and gravity-driven leachate using the zero-tension lysimeters. The gravity-driven leachate includes both diffuse and preferential flow. Soil temperature and water content probes were set to collect data on a 10-min interval during the study period at SF-U, SF-L, and NF-U and on a 1-h interval at TS and NF-L. Lysimeters, soil temperature sensors, and water content probes were installed at two depths within the hillslopes dictated by the shallow soils at the U and L positions of each hillslope: (1) below the majority of the rooting zone of the grasses and shrubs (10 cm) and (2) near the soil–saprolite interface (30 cm). At the TS position where soils are deeper, four lysimeters were installed within the soil profile (5, 10, 30, and 60 cm) to capture the movement of tracer. All lysimeters were installed in September and October 2009, before winter snowfall, so that they would remain *in situ* for 6 months prior to sampling. Nested soil temperature and water content probes are part of the larger BcCZO infrastructure and were installed between July 2009 and April 2010; data reported herein are from the study period only.

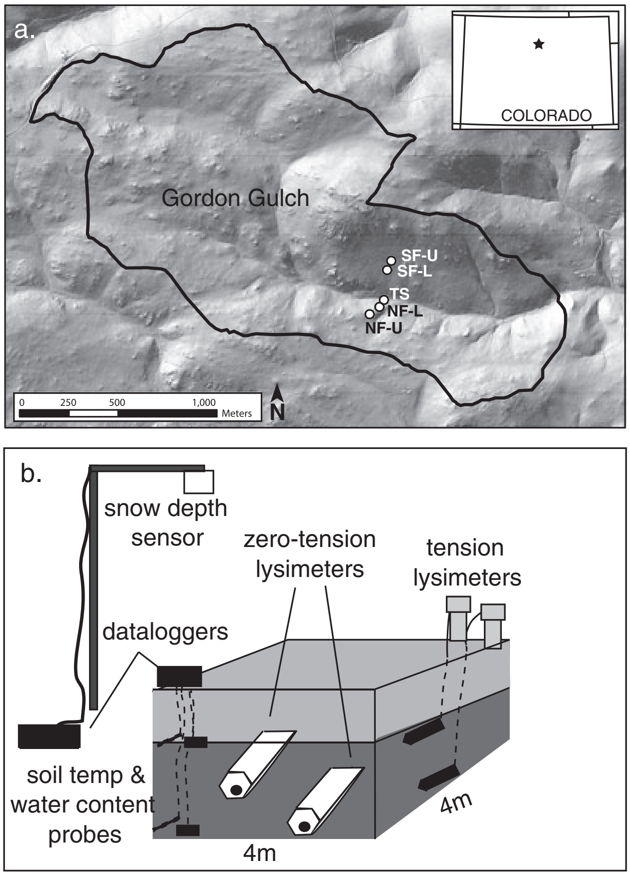

Figure 1. Study area, location of experimental transect, and instrumentation of the plots. (a) LiDAR-shaded relief image for Gordon Gulch, showing location of the experimental plots and (b) nested instrumentation within each study plot. Note that the toeslope plot has additional soil temperature and water content probes and lysimeters at 5 and 60 cm. Inset shows the location of Gordon Gulch within the state of Colorado, USA

Aboveground installations included paired snow depth sensors and air temperature sensors. Within each of the U and L plots, we installed an ultrasonic snow depth sensor (Judd Communications) 1.6–1.9 m above the nested soil temperature and water content probes; snow depth sensors were set to collect data at 10-min intervals.

LiBr tracer studies

We used bromide (applied as LiBr) as a conservative tracer of melt water from the soil–snowpack interface through near-surface soils. On 10 April 2010, during melting of the seasonal snowpack on the north-facing slope, we applied the tracer solution to all plots. At the time of application, there was no snow on the south-facing slope, but there was 0.26 ± 0.06 m of snow on the north-facing slope and toeslope sites (TS). On the south-facing slopes, 2.5 l of tracer solution containing 0.5 M LiBr was applied to the 4×4 m plots at a rate of $0.44\,\mathrm{mm\,h^{-1}}$ for a total application of $6.25\,\mathrm{g\,Br^{-}\,m^{-2}}$. On the north-facing slope, snow was removed from each plot and piled onto a tarp, thereby destroying its internal structure. We applied the tracer solution at the same composition and rate as on the south-facing slope and then shovelled the snow back onto the plots in a uniformly thick layer. The depth of the snowpack was reduced by ~50%, but snow water equivalent (SWE) was preserved. Given that the snowpack was isothermal when we began the experiment (based on snowpack temperature measurements, not shown), we expect that the structural effects on melt water movement were minimal. Several studies have shown that a transition from preferential to matrix flow of melt water through the snowpack is common as accumulated snow ages and warms, lessening the relative importance of snowpack structural features (Colbeck, 1979; Lee *et al.*, 2010; Williams *et al.*, 2010).

Tension lysimeters were immediately evacuated to 40.6 cm Hg of vacuum to begin sampling soil water. We sampled tension lysimeters daily for 40 days, then on an event-basis for an additional two weeks, and collected leachate from zero-tension lysimeters when available. In all, samples were collected over a period of 54 days between 11 April and 3 June 2010. Zero-tension lysimeter samples were used to determine movement of highly mobile water through the subsurface and Br^{-}

DOI: 10.1002/hyp

concentrations of this flow path. Both types of lysimeters were checked and emptied daily, so any samples collected reflect a 24-h period.

Laboratory analysis

All soil solution samples from lysimeters were filtered in the field using 0.45-μm Supor membrane syringe filters (Acrodisc) and stored in 60-ml HDPE bottles. Samples were analysed in the Niwot Ridge Long-term Ecological Research Station's Kiowa laboratory (Boulder, CO, USA) within 1 week of collection. Bromide was measured on a Metrohm 761 Compact Ion Chromatograph (IC) with a detection limit of 0.015 mg l^{-1}.

Snow depth and temperature-index snowmelt models

We constructed two simple models to meet two needs: to fill gaps in the snow depth data caused by periodic measurement failure and low instrument sensitivity at snow depths <10 cm and to estimate a continuous time series of melt water inputs to the subsurface during the spring from our observations of snow depth. This required acknowledging factors that differ strongly between slopes to quantitatively evaluate the differences between the two aspects.

For the snow depth model, the primary snow depth and air temperature observations were collected in the experimental plots at every location except TS during the period of study. We used a precipitation record from the closest NADP station (Sugarloaf, CO94, 39.994°N, 105.48°W, approximately 2.2 km from the study area and at the same elevation) (NADP, 2011) to fill gaps in the snow depth record. The gap correction was achieved by increasing or decreasing snow depth according to the precipitation and air temperature records. We used values of snow density to convert measured precipitation at the Sugarloaf station to snow depth for the gaps in the observational record. Initial snow density (ρ_0) evolved to maximum snow density (ρ_{max}) on each slope (values based on previous observations at the study site). Thus, conversion of precipitation from Sugarloaf was made using

$$P_{snow} = P \times \left(\rho_{water}/\rho_{snow}\right) \times P_{cor} \tag{1}$$

where P_{snow} (mm) is the modified precipitation input (as snow) for modelling the snow depth record, P is measured precipitation (mm water), ρ_{water} and ρ_{snow} are water and snow densities (kg m^{-3}), respectively, and P_{cor} (dimensionless) is an empirical precipitation correction factor that converts the precipitation record from Sugarloaf station (NADP site CO94) to that at Gordon Gulch.

The snowmelt model uses a temperature-index approach that has been employed previously in glacial areas by Hock (1999). Importantly, it incorporates potential clear-sky direct radiation, which serves to reduce the range of error (Ohmura, 2001) and allows us to differentiate the forcing on the two opposing slopes:

$$M = \begin{array}{ll} [(1/n)MF + \alpha_{snow}R_t]T & : T > 0 \\ 0 & : T \leq 0 \end{array} \tag{2}$$

where M is snowmelt rate (mm h^{-1}), MF is a melt factor (mm day^{-1} °C^{-1}), n is the number of time steps per day (here, 24), α_{snow} is a radiation coefficient (m^2 W^{-1} mm h^{-1} °C^{-1}), and T is air temperature (°C). The melt factor and radiation coefficient are determined empirically. R_t is the total radiation (W m^{-2}) calculated for forested regions using the approach of Link *et al.* (2004):

$$R_t = \tau_d R_{d,o} + R_{b,o} e^{-hk_b/\cos\Theta} \tag{3}$$

where t, d, and b refer to total, diffuse, and direct radiation, respectively (with direct radiation modified by slope angle), and o refers to unobstructed locations. τ_d is the transmission coefficient for diffuse radiation through the canopy (dimensionless), h is the canopy height (m), k_b is the extinction coefficient for direct radiation through the canopy (m^{-1}), and Θ is the zenith angle (degrees).

We used measured direct radiation, $R_{b,o}$, from Betasso (40.01°N, 105.34°W, 1934 m elevation), which is another study sub-catchment within the BcCZO. This radiative history was modified for north-facing and south-facing slopes by incorporating both slope angle and orientation (e.g. Hock, 1999). Diffuse radiation, $R_{d,o}$, which is independent of slope angle, is taken from measurements made in Golden, CO, USA, at the NREL Solar Radiation Research Laboratory (SRRL; 39.74°N, 105.18°W, 1829 m elevation) (NREL, 2011) and serves to capture the effects of cloudiness on the melt rate histories.

We optimized the snowmelt model parameters MF and α_{snow} and radiative parameters k_b and τ_d, for conditions on north-facing and south-facing slopes by minimizing the sum of squares for the observed and modelled snow depth record using the Levenberg–Marquardt algorithm.

Soil properties and Hydrus-1D simulations

Disturbed bulk soil samples (sampled as 0–10 and 10–25 cm cores) were collected from the SF-U, TS, and NF-L locations ($n = 1$ per depth, per plot) to characterize unsaturated soil hydraulic properties at upslope and toeslope locations. The samples were repacked to a field-measured bulk density (for each plot) prior to soil hydraulic property analyses. However, the repacking of soil into columns in the laboratory destroyed preferential flow paths, including soil structure and biogenically derived macropores. Saturated hydraulic conductivity (K_{sat}) (m day^{-1}) was estimated using a constant-head permeameter (ASTM, 2011). Soil-water retention curves were measured using the hanging column method (Dane and Hopmans, 2002a), pressure plate apparatus (Dane and Hopmans, 2002b), and a dewpoint potentiometer (Gee *et al.*, 1992). The computer code RETC (van Genuchten *et al.*, 1991) was employed to estimate van Genuchten's (1980) parameters. All samples were processed at the D.B. Stephens and Associates Laboratory, Albuquerque, NM, USA.

DOI: 10.1002/hyp

Numerical simulations of unsaturated flow were conducted with Hydrus-1D (Šimůnek *et al.*, 2008) to further investigate the disparate hydrologic response to snowmelt for the north-facing versus south-facing aspect slopes. An atmospheric boundary condition with surface runoff was used at the top of the domain, using the estimated flux from the snowmelt model. If this flux exceeds the infiltration capacity, then the excess becomes runoff. The boundary condition at the bottom of the domain is free drainage. Finite-element nodal spacing (Δz) was 0.3 cm, and a variable time step (Δt) was used. Parameterization of soil hydraulic properties for both sites uses the van Genuchten (1980) values from Table I using two layers, one from 0- to 10-cm depth and then 10-cm depth to the bottom of the domain, which was the measured depth to saprolite. Saturated hydraulic conductivity in the two-layer system for both slopes was parameterized using the constant-head permeameter values in Table I. Unsaturated hydraulic conductivity was estimated using the Mualem (1976) approach based on the van Genuchten (1980) parameters and the measured K_{sat} values for each site. The initial conditions in the subsurface were specified using the soil-water content data; the 5-cm data were used for 0 to 12.5-cm depth and the 20-cm data was used for 12.5 cm to the bottom of the simulated domain. Simulated soil-water contents were evaluated using the soil-water content observations from the midslope positions on each aspect; these were also the locations for which the snowmelt model fluxes were modelled.

RESULTS

Meteorological forcing

Across the catchment, precipitation during the 2009–2010 water year was 572 mm, with 70% falling as snow. There were nine major snowfall events during the measurement period, with the last snowstorm of the season occurring from 11 through 14 May (Table II). The two slopes had substantial differences in measured air temperature and calculated incoming solar radiation. Mean air temperature on the north-facing slope was 4.2 °C during the period of observations, whereas on the south-facing slope, it was 6.2 °C. In general, the daily highs were higher on the south-facing slope, whereas the lows were lower on the north-facing slope (Figure 2). From about 20 March on, daily mean temperatures were at or above 0 °C and occasionally dropped below 0 °C on both slopes. Similarly, estimated incoming solar radiation (accounting for slope angle and based on incoming radiation data from the Betasso site) was greater (up to ~50%) on the south-facing *versus* the north-facing slope (Figure 3).

The record of measured snow depth (Figure 4) reflects the difference in climatic forcing between the two slopes: the north-facing slope accumulated a seasonal snowpack during the winter and reached its maximum depth on 25 March. The seasonal snowpack disappeared at NF-U and NF-L on 19 April (as determined by daily field observations, which reflect a larger area than the snow depth sensors) but remained until 5 May at TS. In contrast, the south-facing slope did not develop a seasonal snowpack but experienced episodic snow accumulation and melt events throughout the winter and spring (Figure 4).

Table II. Spring 2010 snowstorms at Gordon Gulch during the period of study

Storm date	Duration (days)	SWE (mm)
19 March	1	24
23–24 March	2	35
26 March	1	9
3–7 April	5	9
21–26 April	6	57
28–29 April	2	15
2 May	1	3
6–7 May	2	10
11–14 May	4	49

SWE, snow water equivalent.

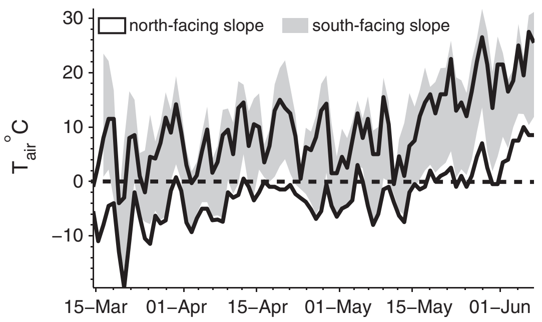

Figure 2. Range in daily air temperatures on the north-facing and south-facing aspects of the study area. Dashed black line marks 0 °C.

Table I. Measured van Genuchten parameters used in the Hydrus-1D model

Location	Depth (cm)	ρ_d (g cm^{-3})	α (cm^{-1})	N (–)	θ_r (cm^3 cm^{-3})	θ_s (cm^3 cm^{-3})	K_{sat} (m day^{-1})
SF-U	0–10	1.14	0.067	1.370	0.007	0.549	4.67
	10–25	1.31	0.037	1.375	0.005	0.399	0.35
TS	0–10	1.09	0.073	1.304	0.000	0.590	1.73
	10–25	1.26	0.058	1.239	0.000	0.447	0.22
NF-L	0–10	0.92	0.068	1.267	0.000	0.629	2.07
	10–25	1.05	0.030	1.310	0.010	0.434	20.74

DOI: 10.1002/hyp

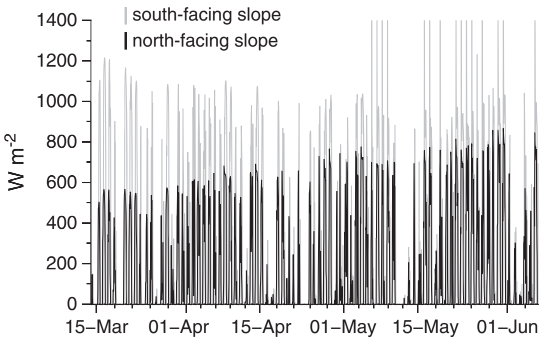

Figure 3. Daily incoming solar radiation estimates (at unit normal vector to the slope) on the north-facing and south-facing slopes. Data are from the Betasso site (40.013°N, 105.340°W, 1934 m elevation).

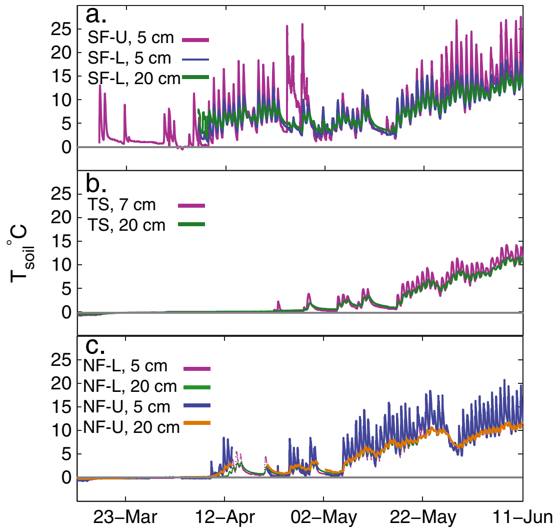

Figure 5. Soil temperature within the soil profile at each plot location across the study transect. Sensors in: (a) south-facing slope plots, (b) toeslope plot, and (c) north-facing slope plots. Solid grey line marks 0 °C.

LiBr tracer studies

When the tracer was applied on 10 April, soil temperatures at north-facing slope locations shifted from around 0 °C to consistently above freezing. South-facing slope plot soils were above freezing well before the start of the experiment (Figure 5).

On the north-facing slope plots (NF-U, NF-L, and TS), Br^- was measured in soil water collected in tension lysimeters at both the 10- and 30-cm depths within 1 to 2 days after tracer application (Figure 6). In these plots, the tracer moved into the subsurface as the seasonal snowpack melted, peaked between 12 and 14 April, and reached a concentration below the detection limit at 30 cm on 23 April at NF-U, 25 April at NF-L, and 29 April at the TS. In the TS plot, we measured breakthrough of the tracer at 60-cm depth on 17 April, 7 days after the tracer application; tracer concentrations remained above the detection limit for a month at this depth, until 19 May.

The pattern of Br^- breakthrough in the south-facing slope plots was very different. The tracer was applied when snow was not present, so it remained on the ground surface until a significant snowstorm (57 mm SWE) occurred from 21 through 26 April. At SF-U, Br^- was first detected in tension lysimeter samples at 10 and 30 cm

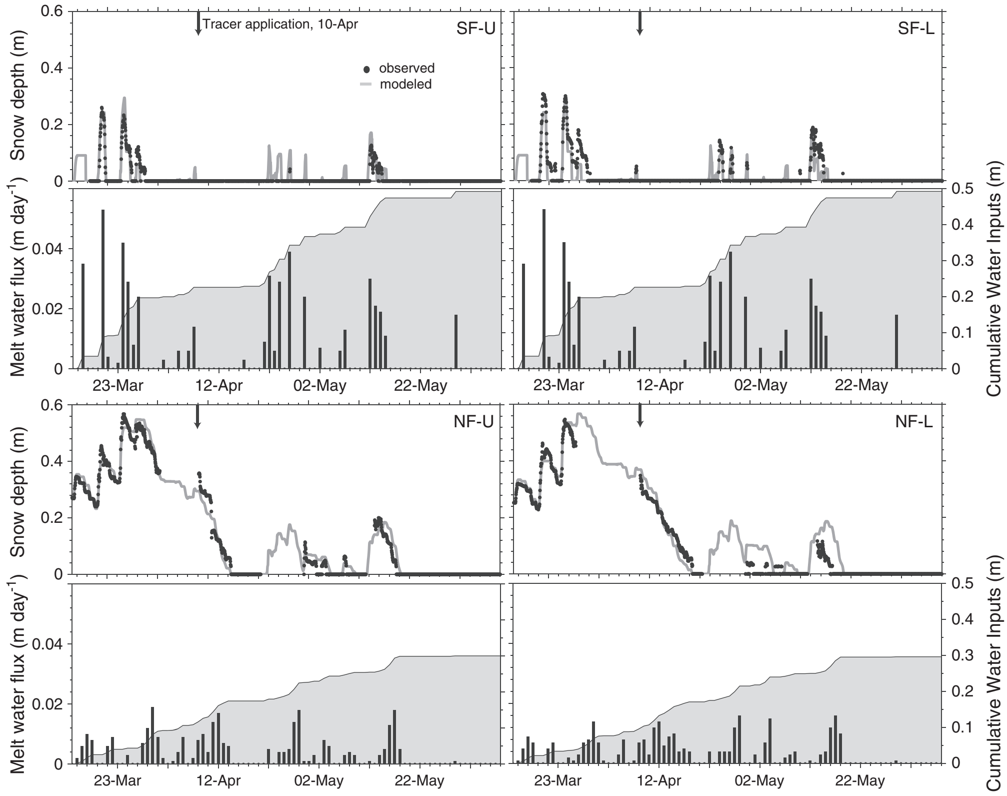

Figure 4. Snow depth and melt water fluxes at four experimental locations (snow depth data were not available for the toeslope location).

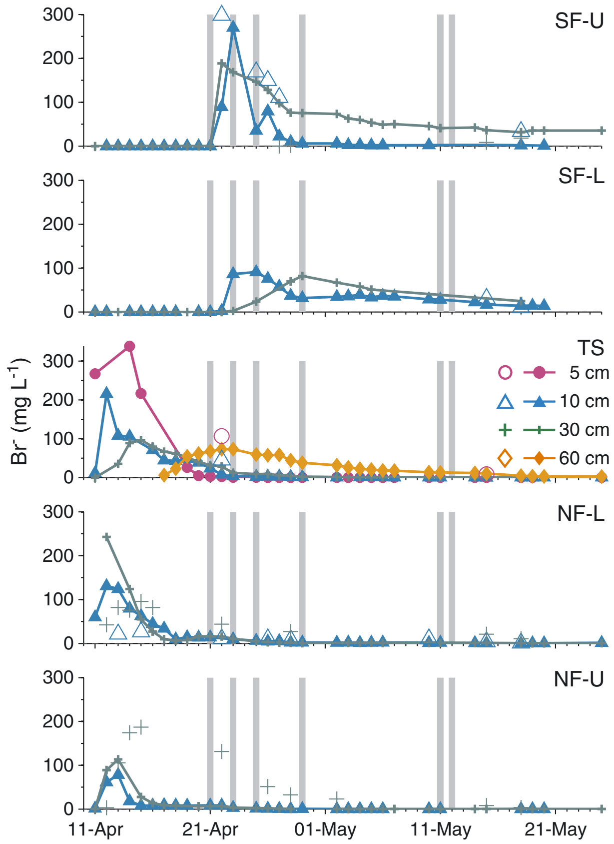

Figure 6. Bromide tracer concentrations in soil water measured in tension lysimeters (closed symbols with lines) and in leachate measured in zero-tension lysimeters (open symbols without lines) at each experimental location. Grey bars mark precipitation events >10 mm snow water equivalent.

on 22 April; it remained above the detection limit until 29 April at 10 cm and did not drop below detection at 30 cm for the duration of the study period. At SF-L, the tracer broke through on 22 and 24 April at 10 and 30 cm, respectively. It remained above the detection limit at both depths for the duration of the study.

Zero-tension lysimeters yielded samples throughout the seasonal snowmelt on the north-facing slope, supporting other lines of evidence for connected flow of water and tracer through the soil matrix during the period of study. In contrast, we collected samples in zero-tension lysimeters on the south-facing slope only following significant (>14 mm SWE) storms, which is also consistent with the pattern of episodic transport of water through the subsurface shown by the soil water (i.e. tension lysimeter) Br^- tracer data (Figure 6). In general, zero-tension lysimeters yielded water with higher Br^-concentrations than tension lysimeters on both slopes, suggesting that they are more reflective of highly mobile water. At SF-L, we did not capture water in zero-tension lysimeters until after the storm on 11 May.

Snow depth and temperature-index melt model results

The snow depth data were similar at both the U and L locations on each slope, so it was only necessary to parameterize the snowmelt model by aspect. Optimization of the model to the snow depth data required MF and α_{snow} (the melt and radiation factors) values that differed greatly between the two slopes: our best-fitting MF was two orders of magnitude larger on the south-facing than the north-facing slope, and α_{snow} differed by one order of magnitude (Table III). Similarly, both optimized radiation parameters associated with the forest cover (k_b and τ_d) reflect greater diminution of incoming direct and diffuse solar radiation on the north-facing than the south-facing slope. The evolution of snow density also differed between the two aspects. We initiated the model with a ρ_0 value of 220 kg m^{-3}, which is typical of low-density snow falling in winter in this climate; on the north-facing slope, it evolved to a ρ_{max} of 650 kg m^{-3}, and to 450 kg m^{-3} on the south-facing slope. These values are within the range measured elsewhere in the study catchment throughout the winter and spring (as deduced from snow depth and SWE measurements; unpublished data). The increase in snow density during the period of interest (values in Table III) mimicked both the ageing of the seasonal snowpack on the north-facing slope and a general increase in the density of snow falling during late-spring storms on both slopes. Regression of observed and modelled snow depth revealed better agreement on the north-facing than the south-facing slope (Figure 7, Table IV); the disconnect between observed and modelled snow depth was primarily after the seasonal snowpack had disappeared, when individual storms accumulated and melted. Cumulative melt water output derived from the temperature-index model was 0.5 m on the south-facing slope, and 0.3 m on the north-facing slope (Figure 4) during the simulation period.

Observed and modelled soil-water dynamics

On the north-facing slope, soil-water content increased rapidly as the seasonal snowpack melted, reached a plateau where it varied in response to late season storms, and then reached a final peak on 17 May (Figure 8). In contrast, on the south-facing slope, soil-water content did

Table III. Parameters for the snow depth and temperature-index models

Aspect	Melt model parameters	Optimized values
South-facing slope (SF-U, SF-L)	ρ_0 (kg m^{-3})	220
	ρ_{max} (kg m^{-3})	450
	Time (day)	20
	MF (mm day^{-1} °C^{-1})	126.6
	α_{snow} (m^2 W^{-1} mm h^{-1} °C^{-1})	1.747×10^{-6}
	k_b (m^{-1})	0.005
	τ_d (dimensionless)	0.9
North-facing slope (NF-U, NF-L)	ρ_0 (kg m^{-3})	220
	ρ_{max} (kg m^{-3})	650
	Time (day)	10
	MF (mm day^{-1} °C^{-1})	9.0
	α_{snow} (m^2 W^{-1} mm h^{-1} °C^{-1})	2.738×10^{-7}
	k_b (m^{-1})	0.06
	τ_d (dimensionless)	0.05

DOI: 10.1002/hyp

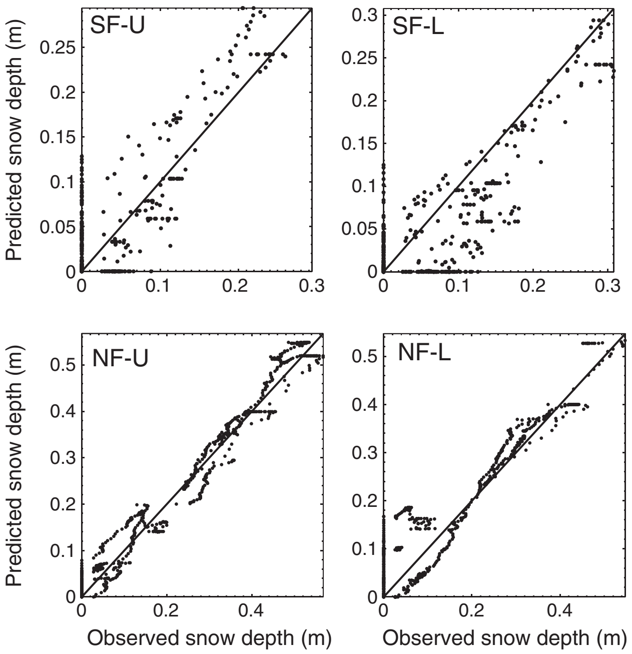

Figure 7. Observed and modelled snow depth values for all plots where snow depth sensors were installed. The 1 : 1 line is shown in each plot.

Table IV. Statistics for the snow depth model

	RMSE	Bias
SF-U	0.0186	0.0026 (25.53%)
SF-L	0.0249	−0.0050 (−28.41%)
NF-U	0.0241	0.0051 (3.90%)
NF-L	0.0428	0.0163 (15.41%)

not experience a sustained wet state (i.e. no steady supply of snowmelt reflected in storage). Increases in soil-water content on the south-facing slope were ephemeral and event driven, following each rapidly melting snowstorm; dry down was more extreme between events, especially in the near-surface (i.e. 5 cm) (Figure 8). Peak soil-water content during the study period occurred on 17 May on the north-facing slope, 3 days after the last spring snow event (Table II), which rapidly melted on both slopes.

Comparison of frequency histograms of soil-water content during the study period from two examples of north-facing and south-facing slope plots (NF-U and SF-U) demonstrates the differences in relative wetness states of the two slopes (Figure 9). Overall, soil-water contents are drier and fall within a narrower range on the south-facing slope (mean of 0.064 and range of 0.068 at SF-U) compared with the north-facing slope (mean of 0.173 and range of 0.241 at NF-U). On the north-facing slope, the values display a bimodal distribution, indicating distinct clusters around the pre-snowmelt period (dry, unshaded) and snowmelt (wet, shaded), see Figure 9; this pattern did not occur on the south-facing slope.

The Hydrus-1D simulation results are shown in Figure 10. Simulated overland flow was zero during the entire simulated period on both slopes. For the north-facing slope, the simulated soil-water contents follow the

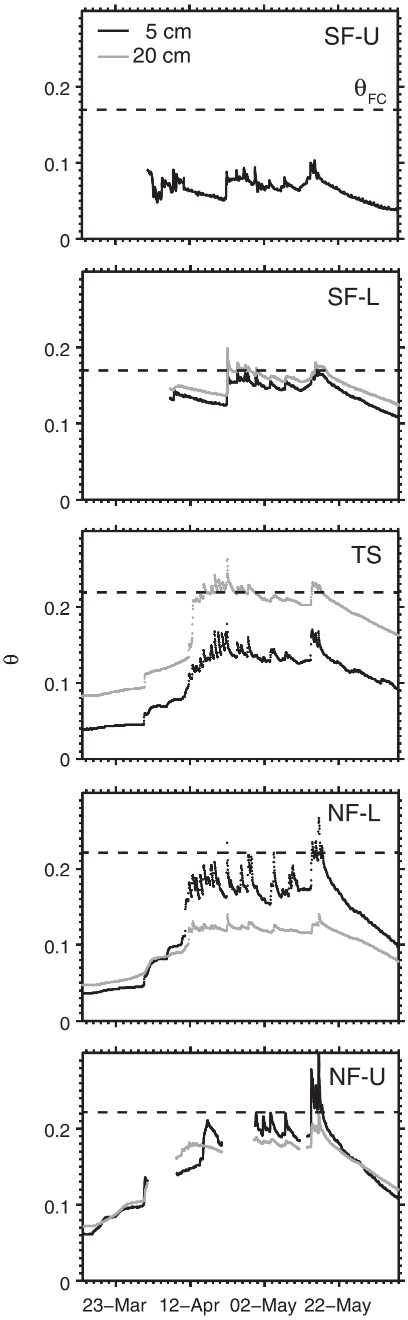

Figure 8. Observed volumetric water content (θ) at all plots

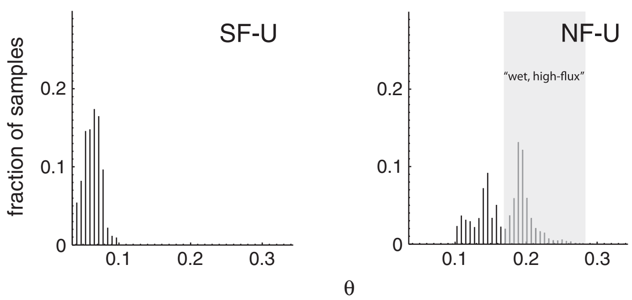

Figure 9. Frequency histograms of volumetric water content data at 5-cm depth for a south-facing and a north-facing plot

same pattern but are much larger than observed at both 5 and 20 cm. In addition, the magnitudes of simulated hydrologic response to events of larger melt flux are overestimated

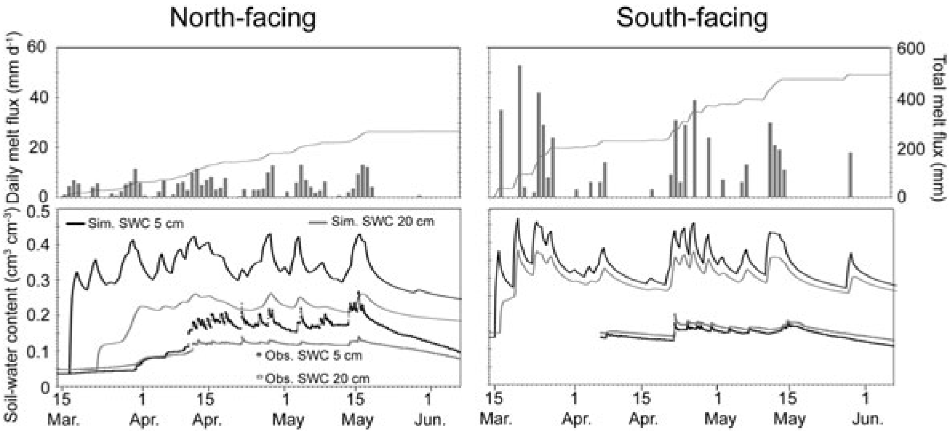

Figure 10. Hydrus-1D simulation results for north-facing and south-facing plots. Simulations are for the lower (i.e. NF-L and SF-L) position on each aspect and shown with accompanying soil-water content observations and melt water fluxes from the temperature-index model.

(Figure 10). South-facing slopes also have larger simulated soil-water contents relative to observed values at 5- and 20-cm depths, and soil-water dynamics in response to melt pulses are overestimated to a greater degree than the north-facing slope. The simulated soil-water contents do capture the observed differences in soil-water content gradients that are present between the aspects (i.e. soil-water content gradients are larger between 5- and 20-cm depth on the north-facing slope compared with the south-facing slope). To investigate the sensitivity of simulated soil-water contents to melt water inputs, we ran a simulation in which 80% of the estimated melt flux was applied as the upper-boundary condition for the north-facing slope. This reduced melt flux scenario reduces the soil-water contents slightly, but does not substantially improve the relative error between simulated and observed soil-water contents on the north-facing slope (results not shown). Based on these simulation results and the minimal sensitivity to melt flux reductions, we suggest that the Hydrus-1D simulations, by not simulating the preferential flow component of unsaturated zone flux, are forcing all of the melt flux to move through the subsurface as matrix flow, thus causing the soil-water contents to be overestimated, in particular on the south-facing slope.

DISCUSSION

The goal of this study was to understand how aspect affects snowmelt dynamics and near-surface hydrologic response in catchments at the rain–snow transition. Our primary methods were to use (1) the LiBr tracer experiments to characterize differences in the timing and transport of melt waters across the north–south catchment cross section and (2) the results from a simple snowmelt model and simulated soil-water content values to further assess the timing of water inputs to the subsurface and resulting subsurface flow paths. Unsaturated flow simulations, driven by the different aspect-driven melt behaviour, were used as supporting evidence for conclusions derived from the tracer and soil-water content data.

The summary of Br^- tracer movement through the subsurface (Figure 6) shows sharp peaks in the concentration data from tension lysimeters for almost all positions along the catchment transect, indicating that primarily vertical, advective transport dominates during the melt season. Flow of water through the subsurface during the period of measurement remained unimpeded by refreezing in the subsurface on both slopes (Figure 5). On the south-facing slope, the differences in the shape of the peak between SF-L and SF-U for soil-water at 10 cm may reflect water sampled from two different domains (Figure 6). It is possible that the dampened peak at SF-L reflects water sampled from a relatively immobile soil-water pool within the matrix, whereas at SF-U, we captured water flowing through the mobile water domain (i.e. preferential flow paths) during the snowstorm on 23 to 24 April. Indeed, our zero-tension lysimeter results support this conclusion: we captured water with high Br^- concentrations at SF-U following events with SWE > 14 mm and not at SF-L until after the storm event on 11 May (Figure 6). The locations of preferential flow paths are controlled by spatially heterogeneous factors, such as soil texture, plant roots, and burrowing animals (e.g. Ghodrati and Jury, 1990; Black and Montgomery, 1991; McIntosh *et al*., 1999), so we may have captured this flow path at only one of the two locations.

The sensitivity of preferential flow to the rate at which water is applied has been observed in several non-snowmelt field studies (e.g. Gjettermann *et al*., 1997; Kasteel, 1997; Perkins *et al*., 2011) and has been clearly presented from synthesized experimental (Nimmo, 2007) and theoretical perspectives (Nimmo, 2010). Although apparent in the zero-tension lysimeter data, these periods of rapid vertical flux were not captured in the soil-water content observations (Figure 8); it is possible that the soil-water content data better reflect soil-water changes in the soil matrix, rather than the mobile domain. We suggest then a departure from the McNamara *et al*. (2005) five-stage model. Rather than the spring 'wet, high flux' phase that they report, we observe a 'dry, high flux' phase on the south-facing slope: near-surface conditions are relatively dry during most of the spring (Figure 9) except

DOI: 10.1002/hyp

for periodic high fluxes caused by activation of highly mobile water flow paths during significant melt events. This result follows recent research reporting activation of preferential flow, even under unsaturated conditions (Nimmo, 2012).

On the north-facing slope, the majority of applied Br^{-} was flushed through the near-surface during the seasonal snowmelt, which lasted 26–42 days along the hillslope profile following the tracer application. Mixing and dispersion of the tracer front in the subsurface likely played a role in controlling the shape of the Br^{-} concentration curves. For example, the Br^{-} peaks at TS flatten with depth through the soil profile; the duration of high Br^{-} concentration at 60 cm is longer, compared with the brief, higher concentration peak (a threefold difference) at 5 cm (Figure 6). In addition, soil-water content of the soil matrix on the north-facing slope responds more to increases in melt water inputs than the south-facing slope, as shown in the soil-water content observations (Figure 10). Thus, on the north-facing slope, we suggest that matrix flow dominates as the transport mechanism, largely due to sustained melt water supply. This pattern more closely reflects the ‘wet, high flux’ stage of the McNamara *et al*. (2005) model than the south-facing slope.

The contrasting melt water dynamics on the two slopes (see Figure 4) have intriguing consequences for soil moisture storage prior to the summer dry season. In alpine and sub-alpine systems, peak soil-water content coincides with the end of the spring snowmelt event (e.g. Molotch *et al*., 2009). Studies such as Bilbrough *et al*. (2000) have shown that high elevation plant species are adapted to initiate growth and nutrient acquisition long before snowmelt ends. At the rain–snow transition, spring snowstorms likely play a similar role in sustaining vegetation communities through the dry summer months, but the pattern of peak soil moisture differs from alpine and sub-alpine systems. On the north-facing slope, we observed an increase in the soil-water content at 5 and 20 cm after the seasonal snowpack had melted, which remained elevated during late April and early May storms (Figure 8); similar results were reported by Geroy *et al*. (2011) for a semi-arid catchment. In contrast, south-facing slope soils were drier throughout the measurement period relative to the north-facing slope (Figures 8 and 9). Similar to Smith *et al*. (2011), our data suggest that the north-facing slope stores water more effectively in the near-surface than the south-facing slope, where water may pass quickly to a deeper weathered bedrock system that isolates it from near-surface evapotranspiration removal. Shifts to earlier snowmelt could change the soil-water storage patterns on the north-facing slopes, which could have larger consequences for the health and composition of the vegetation community.

Our simulations of melt water flux and soil-water content support our observations of different hydrologic response on the two aspects (Figures 4 and 10). The pattern of modelled melt water flux differed greatly between the two slopes, with sustained inputs on the north-facing slope and episodic inputs coinciding with snow events on the south-facing slope. Overall, it showed that more water enters the south-facing than the north-facing slope (Figure 4), which is likely, given more interception by trees and time for sublimation of the snowpack on the north-facing slope. These results align with the timing of simulated and observed soil-water content increases in the subsurface (Figure 10), as well as the immediate response following storms that we observed in the tracer data (Figure 6).

While the temperature-index model results follow our expectations for the general differences between the two aspects – the goal of the modelling exercise – they may not accurately represent the magnitudes of melt flux. Interpretation of melt flux values is limited by an incomplete observational record of snow depth caused by low sensitivity of the sonic snow depth sensors when snowpack is intermittent and an absence of detailed SWE measurements at our experimental plots. Because we used the temperature-index model results as the upper-boundary condition of our Hydrus-1D simulations, it might follow that over-prediction of melt fluxes is the reason for higher simulated than observed values of soil-water content. However, reducing the melt water flux by 20% on the north-facing slope resulted in minimal change to the simulated hydrologic response; the hydraulic conductivity function in Hydrus-1D is highly nonlinear, which causes the hydraulic conductivity to change by a large magnitude for a given change in soil-water content. Instead, we believe that the discrepancy between simulated and observed values arises because (1) our soil-water content observations do not capture preferential flow, so values are low, especially on the south-facing slope, and (2) we used repacked cores to determine the van Genuchten parameters used in Hydrus-1D, so preferential flow was not represented and all water was routed through the matrix, leading to higher simulated values. For the purposes of this study, however, the modelling results are illustrative of the general differences aboveground and belowground on the two slope aspects.

The conceptual model of transport dynamics that we present for the two slopes likely has major implications for biogeochemical cycling of reactive constituents, such as C and N, and lends some insight into how the hydrologic response of these hillslopes may change in response to climatic shifts. On the north-facing slope, longer residence times allowing matrix and event waters to mix in the subsurface may create more opportunities for biogeochemical transformations to occur (e.g. nitrification and inorganic N immobilization; see Stevens *et al*., 1999). On the south-facing slope, only a small fraction of inputs stored within the soil matrix may participate in these biogeochemical pathways, whereas the majority of reactive C and N are transported rapidly to depth with little soil matrix contact (e.g. Bundt *et al*., 2001; Muholland *et al*., 1990). With respect to likely climate change impacts, a shift in temperature could cause a decrease in the amount of precipitation falling as snow, reducing the seasonal snowpack on the north-facing slope. This could change

DOI: 10.1002/hyp

soil moisture storage through the dry summer season, with north-facing slopes becoming either wetter, as all water is forced through the soil matrix, or drier because of more pronounced wetting and drying cycles, similar to the south-facing slope. Clearly, aspect-driven differences in our data sets and the potential changes that may occur under different climate forcing are relevant in these lower elevation catchments at the rain–snow transition and beg further study at the catchment scale.

CONCLUSIONS

Measurement and modelling of point scale snowmelt water fluxes in a forested catchment at the rain–snow transition demonstrate that the timing and fate of snowmelt differs greatly on north-facing and south-facing slopes. North-facing slopes developed a seasonal snowpack, which provided a persistent melt input into the hillslope for 26–42 days after the application of Br^- tracer. In contrast, south-facing slopes did not develop a seasonal snowpack but instead experienced episodic snow accumulation followed by melt events scattered throughout the winter and spring.

LiBr tracer studies and modelling of soil-water content constrain melt water flow paths through near-surface soils, the residence time of melt water, and the degree to which it mixed in the subsurface. On both slopes, the movement of tracer into the subsurface was largely governed by melt water supply, which therefore created the stark contrast between aspects. Soil properties (e.g. texture, organic matter content, and depth to saprolite) that lead to differences in structure (e.g. presence/absence of preferential flow paths) may play an important role in controlling the hydrologic response across the north–south cross section. In future work to test this hypothesis, one could apply liquid water to north-aspect and south-aspect slopes at both high and low rates to determine if aspect-driven preferential flow initiation is the result of inherent differences in soil development or is controlled by supply-rate thresholds driven by aspect-dependent snowmelt timing and rate.

Transport was largely downward, advective flow, with evidence of pore water mixing at the deepest measurement location (60 cm) at the toeslope or near-stream location. We conclude that mechanisms of hydrologic transport differ on the two aspects: the south-facing slope has both periods of rapid vertical flow, initiated by significant snowmelt events, and a relatively immobile matrix storage component indicated by lack of tracer flushing from the soil matrix, whereas the north-facing slope is predominately driven by matrix flow that actively drove tracer-laced water out of the soil domain. Observed soil-water contents support the hypothesis of a wet state, hydrologically connected flow system dominated by vertical matrix flow on north-facing slopes. In contrast, relatively dry soil matrix conditions persist throughout the melt season on the south-facing slopes, suggesting that advective flow supplied by high rates of episodic snowmelt could be bypassing the soil matrix. Our findings underscore the importance of antecedent soil-water content and water input rate as controls on the movement of water in the subsurface during snowmelt, thus leading to differences in hydrologic response by aspect, with potential implications for stream flow contributions, biogeochemical cycling, and weathering processes.

ACKNOWLEDGEMENTS

E. S. H. and R. T. B. were funded by NSF EAR Postdoctoral Fellowships (NSF EAR 0847987 and 0814457) during the study. B. A. E. was funded by a Mendenhall Postdoctoral Fellowship through the National Research Program of the U.S. Geological Survey. Support was also provided by faculty, staff, and students associated with the Boulder Creek CZO (NSF EAR-0724960). We thank Chris Seibold and staff at the Niwot Ridge LTER's Kiowa laboratory for rapid, careful analysis of all samples. We also thank Ola Czastkiewicz, Daniel Eldridge, Hana Fancher, Zan Frederick, Abigail Langston, Christina Pruett, and Nathan Rock for assistance with installation and maintenance of field instrumentation and sampling. In addition, we thank Benjamin Mirus (USGS) and three anonymous reviewers for their helpful comments on this manuscript.

REFERENCES

Anderson RS, Riihimaki CA, Safran EB, MacGregor KR. 2006. Facing reality: Late Cenozoic evolution of smooth peaks, glacially ornamented valleys, and deep river gorges of Colorado's Front Range. In *Tectonics, Climate, and Landscape Evolution*, Willet SD, Hovius N, Brandon MT, Fisher D (eds). Geological Society of America: Boulder, CO, Special Paper 398, Penrose Conference Series; 397–418.

ASTM Standard D2434. 2011. Test method for constant permeability of granular soils (constant head). ASTM International, West Conshohocken, PA. DOI: 10.1520/D2434-68R06.

Bales RC, Molotch NP, Painter TH, Dettinger MD, Rice R, Dozier J. 2006. Mountain hydrology of the Western United States. *Water Resources Research* **42**: W03537. DOI: 10.1029/2008WR007318.

Befus KM, Sheehan AF, Leopold M, Anderson SP, Anderson RS. 2011. Seismic constraints on critical zone architecture, Boulder Creek Watershed, Front Range, Colorado. *Vadose Zone Journal* **10** (3): 915–927.

Bilbrough C, Welker JM, Bowman WD. 2000. Early spring nitrogen uptake by snow-covered plants: a comparison of arctic and alpine plant function under the snowpack. *Arctic, Antarctic, and Alpine Research* **32**(4): 404–411.

Birkeland PW, Shroba RR, Burns SF, Price AB, Tonkin PJ. 2003. Integrating soils and geomorphology in mountains—an example from the Front Range of Colorado. *Geomorphology* **55**: 329–344.

Black TA, Montgomery DR. 1991. Sediment transport by burrowing mammals, Marin County, California. *Earth Surface Processes and Landforms* **16**(2): 163.172.

Broxton PD, Troch PA, Lyon SW. 2009. On the role of aspect to quantify water transit times in small mountainous catchments. *Water Resources Research* **45**: W08427. DOI: 10.1029/2008WR007438.

Bundt M, Jäggi M, Blaser P, Siegwolf R, Hagedorn F. 2001. Carbon and nitrogen dynamics in preferential flow paths and matrix of a forest soil. *Soil Science Society of America Journal* **65**(5): 1529–1538.

Clow DW. 2010. Changes in the timing of snowmelt and streamflow in Colorado: a response to recent warming. *Journal of Climate* **23**: 2293–2306. DOI: 10.1175/2009JCLI2951.1.

Colbeck SC. 1979. Water-flow through heterogeneous snow. *Cold Regions Science and Technology* **1**(1): 37-45.

Cole JC, Braddock WA. 2009. Geologic map of the Estes Park 30′ × 60′ quadrangle, north-central Colorado. U.S. Geological Survey Scientific Investigations Map 3039, 1 sheet, scale 1:100,000, pamphlet, 56pp.

Dane JH, Hopmans JW. 2002a. Hanging water column. In *Methods of Soil Analysis, Part 4—Physical Methods, Soil Science Society of America Book Series No. 5*, Dane JH, Topp GC (eds). Soil Science Society of America: Madison, Wisconsin; 680–683.

Dane JH, Hopmans JW. 2002b. Pressure plate extractor. In *Methods of Soil Analysis, Part 4—Physical Methods, Soil Science Society of America Book Series No. 5*, Dane JH, Topp GC (eds). Soil Science Society of America: Madison, Wisconsin; 688–690.

Dethier DP, Lazarus ED. 2006. Geomorphic inferences from regolith thickness, chemical denudation and CRN erosion rates near the glacial limit, Boulder Creek catchment and vicinity, Colorado. *Geomorphology* **75**(3–4): 384–399.

Erickson TA, Williams MW. 2005. Persistence of topographic controls on the spatial distribution of snow in rugged mountain terrain, Colorado, United States. *Water Resources Research* **41**: W04014. DOI: 10.1029/2003WR002973.

Gee GW, Campbell MD, Campbell GS, Campbell JH. 1992. Rapid measurement of low soil water potentials using a water activity meter. *Soil Science Society of America* **56**: 1068–1070.

van Genuchten MT. 1980. A closed-form equation for predicting the hydraulic conductivity of unsaturated soils. *Soil Science Society of America Journal* **44**(5): 892–898.

van Genuchten MT, Leij FJ, Yates SR. 1991. The RETC code for quantifying the hydraulic functions of unsaturated soils, *EPA/600/2091/065*, Robert S. Kerr Environmental Research Laboratory, Office of Research and Development, U.S. Environmental Protection Agency, Ada, Oklahoma.

Geroy IJ, Gribb MM, Marshall HP, Chandler DG, Benner SG, McNamara JP. 2011. Aspect influences on soil water retention and storage. *Hydrological Processes* Accepted Article. DOI: 1002/hyp.8281.

Ghodrati M, Jury WA. 1990. A field study using dyes to characterize preferential flow of water. *Soil Science Society of America Journal* **54**: 1558–1563.

Gjettermann B, Nielsen KL, Petersen CT, Jensen HE, Hansen S. 1997. Preferential flow in sandy loam soils as affected by irrigation intensity. *Soil Technology* **11**: 139–152.

Grayson RB, Western AW, Chiew FHS, Bloschl G. 1997. Preferred states in spatial soil moisture patterns: local and nonlocal controls. *Water Resources Research* **33**: 2897–2908.

Greenland D. 1989. The climate of Niwot Ridge, Front Range, Colorado, U.S.A. *Arctic and Alpine Research* **21**(4): 380–391.

Haught DRW, van Meerveld HJ. 2011. Spatial variation in transient water table responses: differences between an upper and lower hillslope zone. *Hydrological Processes* **25**: 3866–3877.

Hinckley ES, Kendall C, Loague K. 2008. Not all water becomes wine: sulfur inputs as an opportune tracer of hydrochemical losses from vineyards. *Water Resources Research* **44**: W00401. DOI: 10.1029/2007WR006672.

Hock R. 1999. A distributed temperature-index ice- and snowmelt model including potential direct solar radiation. *Journal of Glaciology* **45**(109): 101–111.

Hogg EH, Hurdle PA. 1995. The aspen parkland in western Canada: a dry-climate analogue for the future of boreal forests? *Water, Air, and Soil Pollution* **82**(1–2): 391–400. DOI: 10.1007/BF01182849.

Kasteel R. 1997. Solute transport in an unsaturated field soil: describing heterogeneous flow fields using spatial distribution of hydraulic properties. PhD thesis, ETH Zurich, Zurich, Switzerland, 108pp.

Lee J, Feng X, Faiia A, Posmentier E, Osterhuber R, Kirchner J. 2010. Isotopic evolution of snowmelt: a new model incorporating mobile and immobile water. *Water Resources Research* **46**. DOI: 10.1029/2009WR008306.

Link TE, Marks D, Hardy JP. 2004. A deterministic method to characterize canopy radiative transfer properties. *Hydrologic Processes* **18**: 3583–3594. DOI: 10.1002/hyp.5793.

Liu F, Williams MW, Caine N. 2004. Source water and flow paths in an alpine catchment, Colorado Front Range, United States. *Water Resources Research* **40**. DOI: 10.1029/2004WR003076.

McIntosh J, McDonnell JJ, Peters NE. 1999. Tracer and hydrometric study of preferential flow in large undisturbed soil cores from the Georgia Piedmont, USA. *Hydrological Processes* **13**: 139–155. DOI: 10.1002/(SICI)1099-1085(19990215).

McNamara JP, Chandler D, Seyfried M, Achet S. 2005. Soil moisture states, lateral flow, and streamflow generation in a semi-arid, snowmelt-driven catchment. *Hydrological Processes* **19**: 4023–4038. DOI: 10.1002/hyp.5869.

Molotch N, Brooks PD, Burns SP, Litvak M, Monson RK, McConnell JR, Musselman K. 2009. Ecohydrological controls on snowmelt partitioning in mixed-conifer sub-alpine forests. *Ecohydrology* **2**: 129–142.

Mualem Y. 1976. A new model for predicting the hydraulic conductivity of unsaturated porous media. *Water Resources Research* **12**: 513–522.

Muholland PJ, Wilson GV, Jardine PM. 1990. Hydrogeochemical response of a forested watershed to storms: effects of preferential flow along shallow and deep pathways. *Water Resources Research* **26**(12): 3021–3036.

NADP. 2011. [Data available online: http://nadp.sws.uiuc.edu/data/. Accessed 22 June 2011.]

Nimmo JR. 2007. Simple predictions of maximum transport rate in unsaturated soil and rock. *Water Resources Research* **43**: W05426.

Nimmo JR. 2010. Theory for source-responsive and free-surface film modeling of unsaturated flow. *Vadose Zone Journal* **9**: 295–306.

Nimmo JR. 2012. Preferential flow occurs in unsaturated conditions. *Hydrological Processes* **26**(5): 786–789.

NREL. 2011. [Data available online: http://www.nrel.gov/midc/srrl_bms/. Accessed 1 May 2011.]

Ohmura A. 2001. Physical basis for the temperature-based melt-index method. *Journal of Applied Meteorology* **40**: 753–761.

Peet RK. 1981. Forest vegetation of the Colorado Front Range. *Vegetatio* **45**: 3–75.

Perkins KS, Nimmo JR, Rose CE, Coupe RH. 2011. Field tracer investigation of unsaturated zone flow paths and mechanisms in agricultural soils of northwestern Mississippi, USA. *Journal of Hydrology* **396**: 1–11.

Phillips RW, Spence C, Pomeroy JW. 2011. Connectivity and runoff dynamics in heterogeneous basins. *Hydrological Processes* **25**: 3061–3075.

Rood SB, Pan J, Gill KM, Franks CG, Samuelson GM, Shepherd A. 2008. Declining summer flows of Rocky Mountain rivers: changing seasonal hydrology and probably impacts on floodplain forests. *Journal of Hydrology* **349**: 397–410.

Smith TJ, McNamara JP, Flores AN, Gribb MM, Aishlin PS, Benner SG. 2011. Small soil storage capacity limits benefit of winter snowpack to upland vegetation. *Hydrological Processes* **25**: 3858–3865.

Steinweg JM, Fisk MC, McAlexander B, Groffman PM, Hardy JP. 2008. Experimental snowpack reduction alters organic matter and net N mineralization potential of soil macroaggregates in a northern hardwood forest. *Biology and Fertility of Soils* **45**: 1–10. DOI: 10.1007/s00374-008-0305-3.

Stevens DP, Cox JW, Chittleborough DJ. 1999. Pathways of phosphorus, nitrogen, and carbon movement over and through texturally differentiated soils, South Australia. *Australian Journal of Soil Research* **37**: 679–693.

Stewart IT, Cayan DR, Dettinger MD. 2004. Changes in snowmelt runoff timing in Western North America under a 'business as usual' climate change scenario. *Climatic Change* **62**(1–3): 217–232. DOI: 10.1023/B:CLIM.0000013702.22656.e8.

Stieglitz M, Shaman J, McNamara J, Engel V, Shanley J, Kling GW. 2003. An approach to understanding hydrologic connectivity on the hillslope and the implications for nutrient transport. *Global Biogeochemical Cycles* **17**(4). DOI: 10.1029/2003GB002041.

Šimůnek J, van Genuchten MT, Šejna M. 2008. Development and applications of the HYDRUS and STANMOD software packages and related codes. *Vadose Zone Journal*. DOI: 10.2136/vzj2007.0077.

USDA. 2009. Custom Soil Resource Report for Arapaho-Roosevelt National Forest Area, Colorado, Parts of Boulder, Clear Creek, Gilpin, Grand, Park and Larimer Counties, Gordon Gulch. United States Department of Agriculture. 24pp.

Williams MW, Brooks PD, Seastedt T. 1998. Nitrogen and carbon soil dynamics in response to climate change in a high-elevation ecosystem in the Rocky Mountains, U.S.A. *Arctic and Alpine Research* **30**(1): 26–30.

Williams MW, Barnes RT, Parman JN, Freppaz M, Hood E. 2011. Stream water chemistry along an elevational gradient from the Continental Divide to the Foothills of the Rocky Mountains. *Vadose Zone Journal* **10**: 900–914.

Williams CJ, McNamara JP, Chandler DG. 2009a. Controls on the temporal and spatial variability of soil moisture in a mountainous landscape: the signature of snow and complex terrain. *Hydrology and Earth System Sciences* **13**: 1325–1336.

Williams MW, Seibold C, Chowanski K. 2009b. Storage and release of solutes from a subalpine seasonal snowpack: soil and stream water response, Niwot Ridge, Colorado. *Biogeochemistry* **95**: 77–94.

Williams MW, Erickson TA, Petrzelka JL. 2010. Visualizing meltwater flow through snow at the centimetre-to-metre scale using a snow guillotine. *Hydrological Processes* **24**: 2098–2110. DOI: 10.1002/hyp.7630.

WRCC. 2011. [Data available online: http://www.wrcc.dri.edu/cgi-bin/cliGCStT.pl?co3629. Accessed 22 June 2011.]